RSC Advances

PAPER

View Article Online
View Journal | View Issue

Cite this: *RSC Adv.*, 2021, **11**, 5035

Effective oil–water mixture separation and photocatalytic dye decontamination through nickel-dimethylglyoxime microtubes coated superhydrophobic and superoleophilic films†

Jinxiu Ma,[a] Wen Meng,[a] Lahong Zhang,[a] Feng Li *[ab] and Taohai Li *[ab]

Oils and solvable organic pollutants in wastewater demand separations of the components along with efficient photocatalysis in water treatment. Herein, we report on a practical purification strategy by using the multifunctional nickel-dimethylglyoxime [Ni(DMG)$_2$] microtubes to separate the liquid mixture and degrade organic pollutants. The self-assembled [Ni(DMG)$_2$] tubes was synthesized by a facile co-precipitation method. The static contact angle of the film prepared by mixing [Ni(DMG)$_2$] powder (1 : 2 wt%) into polydimethylsilicone (PDMS) to water can reach 161.3°, which can still remain superhydrophobic but oil-friendly under corrosion conditions. PDMS imparts good mechanical properties and serves as both the adhesive and hydrophobic material. PFOTS methanol solution contains a large number of low surface energy groups, which can reduce the surface free energy of [Ni(DMG)$_2$] rough structure. The superhydrophobic rough surface prepared by hollow micron tubular [Ni(DMG)$_2$] samples must have both low surface energy substance and hollow micron tubular morphology. Due to the unique wettability, oil and water were efficiently separated from the oil–water mixture through the films. The coated film itself is photocatalytic in degrading quinoline blue, rhodamine B, methyl orange and methylene blue. By using the film's multifunctionality, a practical wastewater treatment was realized *via* water–oil separation, followed by fast photocatalytic degradation of solvable dyes.

Received 30th October 2020
Accepted 18th January 2021

DOI: 10.1039/d0ra09240a

rsc.li/rsc-advances

Introduction

Among numerous methods for water purification, photocatalytic techniques distinguish themselves from their peers thanks to their multiple functions in sewage treatment, atmosphere purification and sun useage.[1–4] However, they suffer from several deficiencies in practical applications. Besides low catalytic efficiency, a disadvantage of current photocatalysts stems from high aqua solubility, setting obstacles in recoveries and reuses of the catalysts. Furthermore, wastewater is frequently associated with large amount of oils either from industry, fracking, or due to crude oil spillages.[5–7] The hazardous water–oil mixture poses even larger challenges in water treatments. Hence, chemicals with only catalytic properties can hardly accomplish direct sewage treatments where oil–water mixture still remains in liquid forms after physically removing the sediments. Thus, ideal photocatalysts should be equipped with unique wettability along with their chemically efficient, environmentally friendly, and generally usable merits. For these reasons, superhydrophobic surfaces were engineered to help catalyst recycles, where special wetting properties the synthetic chemicals after photochemical reactions.[8–11] Coatings with superhydrophobic materials have also been coated for a variety of films to enhance anticorrosive protection against ambience liquids or other corrosives for photocatalysts.[12,13] Despite these successes in hydrophobic designs for photocatalysts, however, methods to produce superhydrophobic surfaces are complicated and expensive, yet limiting large-scale manufactory. Furthermore, separation of oil–water mixtures remains impossible just through hydrophobic surfaces, where the oil may also be repelled simultaneously. Thus, in addition to high catalytic ability of the synthetic chemicals, an ideal photocatalytic system demands tailored oil/water wettability which can be reached with facile coating techniques.

If it has both photocatalytic activity and oil–water separation ability, the coordination complex can undertake multifunctional tasks in actual photocatalytic water treatment. For example, the dimethylglyoxime ($dmgH_2$) based coordination complexes are found useful as enzymes[14] and catalysts[15] along with their conventional function as reagent for Ni(II) ions.[16,17] Reaction principle originates from complexation between

[a]*College of Chemistry, Key Lab of Environment Friendly Chemistry and Application in Ministry of Education, Xiangtan University, Xiangtan, 411105, China. E-mail: fengli@xtu.edu.cn; hnlth@xtu.edu.cn*

[b]*Nano and Molecular Systems Research Unit, University of Oulu, P.O. Box 3000, FIN-90014, Finland*

† Electronic supplementary information (ESI) available. See DOI: 10.1039/d0ra09240a

quantitative Ni^{2+} and dimethylglyoxime, followed by production of bright red $[Ni(DMG)_2]$ chelates.[18] The reaction scheme was also developed where positioning of $[Ni(DMG)_2]$ atoms in molecular structure and position of hydrogen in hydrogen bonding were amended.[19,20] Even though a heterogeneous catalyst of nickel-dimethylglyoxime/ZSM-5 Zeolite was reported with high degradation efficiency of methyl green under UV irradiation,[21] the degradation efficiency of $[Ni(DMG)_2]$ particles out of zeolite framework did not show considerable performance. As for the synthesis, single crystal 1-D $[Ni(DMG)_2]$ microrods/tubes were realized by water bath or other methods, while highly selectively visual detection of Ni^{2+} seen in test strips. Morphologies can be well controlled through operating the reaction kinetics by adjusting reaction conditions, so that the shape of the formed microstructure would be simply adjusted from the microrod to the microtube.[22] In addition, in the field of hydrogen production by water splitting, it is reported that a novel material consisting of black phosphorus (BP) and nickel-dimethylglyoxime nanorods was successfully prepared *via* a facile *in situ* calcination strategy, which possesses efficient catalytic activity for hydrogen production from water splitting.[23] Despite above functionality of $[Ni(DMG)_2]$ and its potentials in preparation of Ni/NiO nanoparticles,[24–26] the multifunctional properties of $[Ni(DMG)_2]$ to fit sewage treatment have never been revealed. Indeed, to enable special surface wettability, screen-printing the as-prepared nanocomposite is advanced in low cost, time efficiency, facial process, easy operation and intriguing potential applications in different industries. It has been successfully adopted to fabricate superconducting tape[27] or superhydrophobic/superoleophilic films.[28] In such a context, engineering the $[Ni(DMG)_2]$ to form photocatalytic and superhydrophobic/superoleophilic properties may further extend the screen-printing technology in practical sewage treatment besides its applications in oil/water separations.[29–32]

In this work, we developed a simple precipitation method to prepare photocatalytic $[Ni(DMG)_2]$ hollow microtubes. They were screen-printed on different substrates to reach high recyclability, easy operability, low cost and environmental protection. As shown in Table S1.† The as-prepared $[Ni(DMG)_2]$ films not only exhibit excellent photocatalytic properties but also exhibit excellent stability and reusability compared with transition metal complex-based catalysts such as MnV_2O_6 (ref. 33) or Ag_3PO_4.[34] Furthermore, the as-prepared $[Ni(DMG)_2]$ films also exhibited superhydrophobicity and superoleophilicity. The hydro- and oleo-wettability gifts films powers of splitting oil–water mixtures. We also rationalize a procedure for wastewater purification, where contaminated water in oil–water mixture was firstly flitted, and further decontaminated through photocatalysis coated substrates. Results show that purified water was successfully obtained by using the $[Ni(DMG)_2]$ film as the filter and photocatalyst.

Experimental section

Materials

Nickel chloride hexahydrate, dimethylglyoxime, sodium hydroxide, anhydrous ethanol, anhydrous methanol, *n*-octane, 1*H*,1*H*,2*H*,2*H*-perfluorodecyltriethoxysilane (PFOTS) and polydimethylsiloxane (PDMS) were obtained from China, and all reagents are analytical grade. The glass substrates (1 cm × 1 cm, 4 cm × 6 cm) were obtained locally. They were carefully cleaned with dimethyl ketone, absolute ethyl alcohol and pure water under ultrasound conditions in fifteen minutes, sequentially, in the stove at 70 °C until drying.

Preparation and characterization of $[Ni(DMG)_2]$

The synthesis of $[Ni(DMG)_2]$ was performed by the facile precipitation method. In a typical process, $NiCl_2 \cdot 6H_2O$ (0.1 g) was completely liquefied in pure water (100 mL) under the condition of continually magnetic stirring and 70 °C water bath heating. Afterwards, dimethylglyoxime (0.3 g) was dissolved in anhydrous ethanol (30 mL). The step was followed by dripping dimethylglyoxime ethanol solution into the $NiCl_2 \cdot 6H_2O$ solution. Adjusting the pH of the mixture to 8 was to use a 1 mol L^{-1} NaOH solvent under continuous stirring. The solution was constantly mixed in thirty minutes of 70 °C under water bath condition to form the red suspension. After that, the sample was gathered with filtration and cleaned by 20 mL of pure water with repeatedly. The powder product was dried at 100 °C for 12 h in a vacuum oven for characterization.

X-ray diffraction (XRD) measurements were conducted from 5° to 80° on a Bruker D8 ADVANCED diffractometer (Cu-Kα, λ = 0.15406 nm; 40 kV; 40 mA) with a step of 0.02°. The surface morphology evolution was measured by JSM-6610LV scanning electron microscope (SEM) with accelerating voltage of 30 kV, 200 kV JEM-2100F transmission electron microscope (TEM) and energy dispersive X-ray spectrometer (EDS). Thermogravimetric analysis (TGA) was done under Ar aura in the scanning state of 10 °C min^{-1} from 50 °C to 600 °C using a Shimadzu TGA-50 thermogravimetric analyser. FTIR spectra were noted using Fourier transform spectrometer (Nicolet 6700) in the region of 4000–500 cm^{-1}, and the ultraviolet visible diffuse reflectance spectrum was recorded using an ultraviolet-visible spectrophotometer (UV 2550, Shimadzu, Japan).

Photocatalytic activity of $[Ni(DMG)_2]$ films under UV light irradiation

$[Ni(DMG)_2]$ films were fabricated by skilled screen-printing technology. Typically, $[Ni(DMG)_2]$ dust was mixed (1 : 2 wt%) into polydimethylsilicone (PDMS), then that mixture was brushed onto a glass (4.0 cm × 6.0 cm) through sieved screen to form a film. Then the whole prepared film was fixed to a film at indoor temp until it was dried.

Photocatalytic activities of that as-prepared $[Ni(DMG)_2]$ film was assessed through degradaing quinoline blue, rhodamine B, methyl orange or methylene blue below ultraviolet light. Specifically, 50 mg of the sample powder was added into 100 mL 5 mg L^{-1} QB solution and stirred in dark for 30 min to reach the absorption–desorption equilibrium. After turning on the light, 3 mL of the reactive solution was drawn out every 20 min. The source of the UV lamp is a 300 W high pressure mercury lamp, at the same time, the powder in the container illuminated by the UV lamp is ten centimeters from the lamp. Dyes changes in

the absorption spectra were recorded by measuring the maximal absorption peaks of the dyes using a UV-vis spectrophotometer (Cary 100, Agilent).

Wetting behavior tests with surfaces modified [Ni(DMG)$_2$]

The superhydrophobic surfaces were prepared *via* the same technological process as to the one for [Ni(DMG)$_2$] films implemented in photocatalytic activities experiment. To get liquid permeability, filter paper, filter cloth, copper grid and iron mesh were employed as substrates along with the 1 cm × 1 cm glass plate. After that, a few drops of a 2% (v/v) PFOTS methanol solution was gently added to the film made of the glass plate as a substrate and completely covered on the film. Therefore, the surface energy of the surface construction of the film is lowered to thereby improve the hydrophobic properties. Injection syringe was used to fetch methanol solution of 2% (v/v) PFOTS dripped on the prepared films to ensure the film surfaces wetting. Then, a [Ni(DMG)$_2$] covered film based on a glass plate was cured to form a film at room temp until it was dehydrated.

The water contact angle (CA) was measured using an instrument of the Raméhart model p/n 250-F1. Pure water (10 μL) was gently dripped to the prepared film with a syringe. The contact angle numbers were averaged through calculating the CAs at five different locations on the same membrane.

Results and discussion

Fig. 1A shows the ball-and-stick model of [Ni(DMG)$_2$]. Red, light gray, dark gray, purple and green spheres represent O, H, C, N and Ni atoms, respectively. Fig. 1B depicts the experimental XRD structure diagram from the synthetic sample along with simulated one by applying crystals datum from analyzing monocrystal construction. The shape of the peak in the XRD pattern is acute and limited, indicating that the product has well degree of crystallization. It was observed that the XRD pattern of the synthesized [Ni(DMG)$_2$] (Fig. 1B(b)) was also consistent with the simulation results (Fig. 1B(a)), as given by ref. 32. The product belongs to pure orthorhombic space group of [Ni(DMG)$_2$] with lattice constants of $a = 1.657$, $b = 1.042$, $c = 0.647$ nm. The diffraction peaks and intensities of the most dominant peaks in the XRD pattern are the same as in the ref. 19, 35 and 36. In addition, (002), (112), (240) and other crystal planes are also consistent with values in literature. No additional peaks were found in the patterns, proving the purity of the as-prepared [Ni(DMG)$_2$] powders.

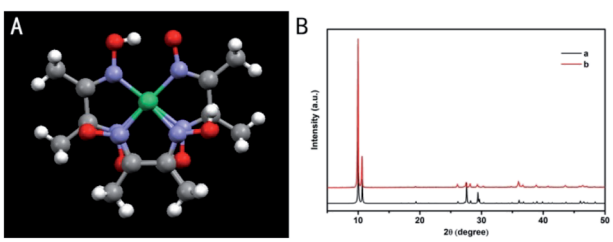

Fig. 1 (A) The structure of Ni(DMG)$_2$; (B) simulated (a) and experimental XRD patterns (b) of the as-synthesized [Ni(DMG)$_2$] product.

The SEM images in Fig. 2A(a) and (b) present crystalized [Ni(DMG)$_2$] microtubes, and (c) and (d) the TEM images of synthetic microtubes of an individual microtube. With mean size of about one μm, wall width of about 0.5 μm and length of 10 μm, the microtubes are found hollow as viewed in higher magnified images. A possible formation scheme to the morphology is proposed as follows. In turn, it undergoes the processes of nucleation, crystal growth and self-assembly growth. First, a solution of $NiCl_2 \cdot 6H_2O$ and a $C_4H_8N_2O_2$ solution was mixed to form an amorphous particle of [Ni(DMG)$_2$], which was used as a precursor of the crystals. During the synthesis of the water bath, the molecule nucleate and nanonize. Since a single molecule of [Ni(DMG)$_2$] has a sheet structure with very high surface free energy, the sheet stacks to molecular crystals readily along the *c*-axis, while growths along the *a*- and *b*-axis are relatively slow. Consequentially, the [Ni(DMG)$_2$] crystal tends to be microrods.[37] Under the action of static electricity and under the condition of minimizing the gross system energy under alkaline conditions, the microrods amalgamated according to certain rules during the reaction process, forming the microtubes.[38] The HRTEM results further demonstrate the successful composition of [Ni(DMG)$_2$] (Fig. 2A(e) and (f)). Chemical components of the as-prepared [Ni(DMG)$_2$] were further studied through energy dispersive X-ray spectroscopy (EDS). As shown in Fig. 2B, characteristic X-ray emissions from C, O, N and Ni were identified.

The thermal stability of as-prepared powder was studied using thermal gravimetric analysis (TGA) as shown in Fig. S1.†

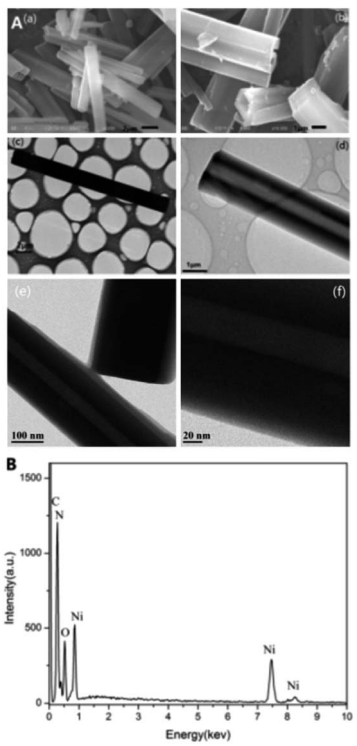

Fig. 2 SEM images, TEM, HRTEM images and EDS analysis of [Ni(DMG)$_2$]. (A) (a) Low-magnification, (A) (b) high-magnification SEM images, (A) (c and d) TEM images and (A) (e and f) HRTEM images of the [Ni(DMG)$_2$]; (B) EDS analysis of [Ni(DMG)$_2$].

In the first stage, the as-prepared sample endures a continuous mass loss of 10% between the temperature of 50 °C and 250 °C due to the dehydration of the material. A second weight change was observed between the temperature of 250 °C and 300 °C with a mass loss of 74.20%, according to the theoretical weight loss of 74.15%. This also demonstrated that $[Ni(DMG)_2]$ was the product and it decomposed at 250 °C.

The FTIR spectrum of $[Ni(DMG)_2]$ is presented in Fig. S2.† The O–H tensile chatte of the absorbed water molecules resulted in a wide peak with a peak of 3354 cm^{-1}. A weak band at 1790 cm^{-1} indicates a strong intramolecular hydrogen bonding in the $[Ni(DMG)_2]$ complex. Other characteristic absorption peaks of 1571 cm^{-1}, 1367 cm^{-1} and 1234 cm^{-1} are attributed to the C=N stretching mode, N–OH bending vibration and N–O stretching modes, respectively.[39] Furthermore, the absorption band at 1115 cm^{-1} is related to the C–O tensile shaking of the trace amount of ethanol collected in the $[Ni(DMG)_2]$[40] microtube, and the absorption peak at 990 cm^{-1} may be due to C–H curve shaking. All the above features prove the formation and structure of $[Ni(DMG)_2]$.

Electronic structures of semiconductor catalysts are of crucial importance for the materials photocatalytic functions. For this reason, the electronic structure of $[Ni(DMG)_2]$ was investigated through the UV-vis diffuse reflectance spectroscopy. As can be seen in Fig. S3(A),† $[Ni(DMG)_2]$ presents an intense absorption with the edge at the wavelength near 680 nm, corresponding to its characteristic energy gap value of approximately 1.82 eV through the theoretical calculation. Beside the peak in the UV region, a strong absorption peak at 600 nm indicates a possible application of the material as a superior visible light photocatalyst.

In addition, a Mott–Schottky curve was obtained in the electrochemical test. The Mott–Schottky curve is used to further reveal the structural features of $[Ni(DMG)_2]$ (Fig. S3(B)).† It is observed that due to the positive slope of the linearity diagram, $[Ni(DMG)_2]$ can be attributed to the n-type semiconductor. Therefore, its flat band is −0.25 eV and the conduction band is −0.03 eV (*vs.* NHE). At the same time, the valence band is calculated by its characteristic energy gap value to be 1.79 eV.

The photocatalytic activity of the successfully synthesized powder was tested through degrading the typical organic contaminant quinoline blue using radiation with a UV lamp. Prior to photocatalytic degradation, a set of blank controls was first prepared, and the quinoline blue solution (5 mg L^{-1}, 100 mL) was subjected to ultraviolet degradation without addition of the already synthesized sample. After 120 minutes of exposure to ultraviolet light, the degradation effect indicated that quinoline blue did not decompose. In contrast, with that existence of $[Ni(DMG)_2]$ powder (0.5 g L^{-1}), 32.6% of dye discoloration was reached after 2 hours of UV radiation (Fig. S4†). The reason for this inferior efficiency of dye degradation maybe due to a hollow tubular structure of $[Ni(DMG)_2]$ with lighter powder size floating in the dye solution. Magnetic stirring can't make it evenly dispersed in the dye solution leading to hindering the absorption of light so that the efficiency of dye degradation with $[Ni(DMG)_2]$ is unsatisfactory. The $[Ni(DMG)_2]$ was also printed on a 4 × 6 cm^2 glass plate by using screen-printing technique. Before irradiation with UV light, the glass panels were placed in dye solution carried out adsorption. When the photocatalyst reaches the adsorption–desorption counterpoise, the consistence of quinoline blue doesn't transform any more with the reaction time. As shown in Fig. 3, the characteristic absorption peak of the dye decreased gradually with retention time, and reached 91% of degradation rate after 120 min.

The experiments were then extended by using multiple kinds of colored organics as contaminants. Fig. 4a–c display the time evolution of the spectra during the degradation of rhodamine B, methyl orange and methylene blue (5 mg L^{-1}, 100 mL). Fig. 4d shows the concentration changes of rhodamine B, methyl orange and methylene blue (C/C_0), where the absorption peaks decreased gradually with the retention time. After two hours of irradiation, degradation efficiency of these three dyes reached to 58%, 40% and 74%, respectively. It can be concluded that $[Ni(DMG)_2]$ has selective photocatalytic abilities for degrading quinoline blue and methylene blue.

It has been noticed that hollow microtubes may have unique wettability thanks to their morphological merits.[41] Here the product structure in Fig. 2A(b) may behave similarly. For this reason, the water contact angle (CA) on that $[Ni(DMG)_2]$ film was appraised by using 10 μL water droplets (pH = 7). The CA value about the glasses plate-based film modified with 2% (v/v) PFOTS in methanol was appraised. Fig. 5a shows the mean value of CA on the glass substrate of the control group without filming. An angle of 64° was obtained, referring to the hydrophilicity of the glass substrates. The CA number was increased to 93° after treatment with the PFOTS (Fig. 5b). In contrast, on the $[Ni(DMG)_2]$-coated glass, the CA value was determined to 161.3° (Fig. 5c), denoting the superhydrophobicity of the film. In Fig. 5d, we dipped the coated glass into a 5 wt% NaCl solution for ten minutes. Thereafter, the coating was allowed to air dry at ambient temp for twenty four hours, and then water contact angle was measured. The sample had a CA value of 157.2°, still keeping the superhydrophobicity. The corrosion reaction from 5 wt% NaCl compound doesn't change the superhydrophobic surface formed by the $[Ni(DMG)_2]$ samples.

The physical mechanism of superhydrophobicity is also investigated. According to the Cassie–Baxter model, the

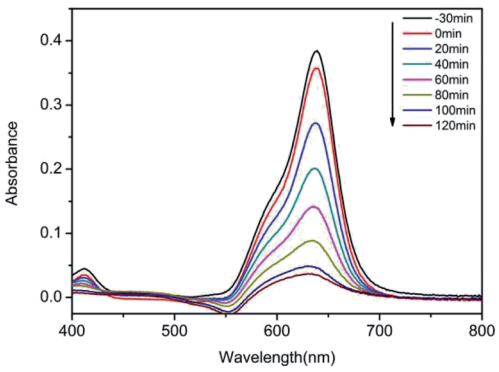

Fig. 3 Time evolution of the spectra during the photodegradation of quinoline blue mediated under UV light irradiation.

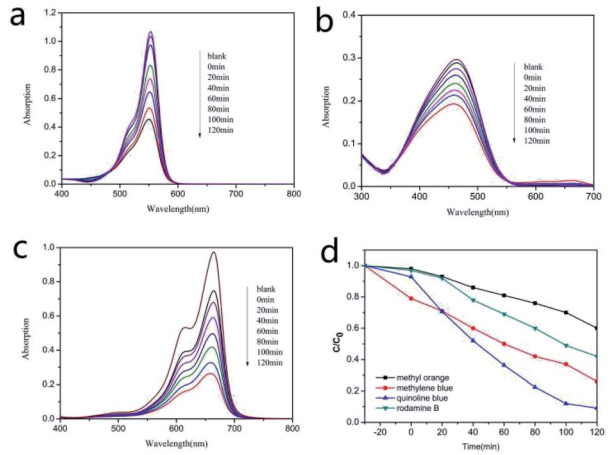

Fig. 4 $[Ni(DMG)_2]$ time evolution of spectra during photodegradation of Rhodamine B (a), methyl orange (b), methylene blue (c) by coating; (d) the concentration changes of rhodamine B, methyl orange, methylene blue and quinoline blue (C/C_0).

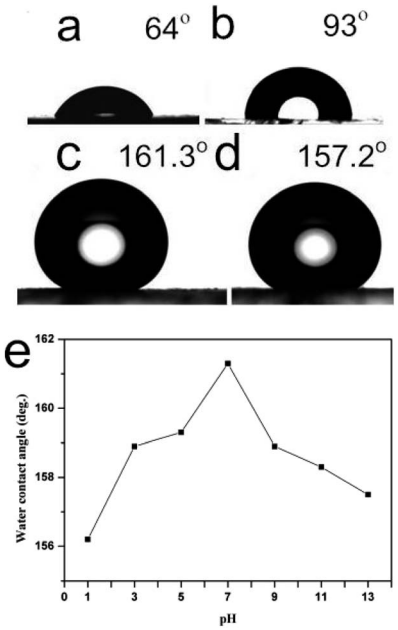

Fig. 5 Water contact angles of (a) glass, (b) treated with 2% (v/v) PFOTS, (c) treated with a dilute $[Ni(DMG)_2]$ and 2% (v/v) PFOTS, (d) aqueous solution of NaCl, (e) the modified prepared surface according to the pH values of the water droplet.

superhydrophobic property is that the droplets form tiny air bubbles above the coarse cover, forming a recombination interphase. In this work, hollow tubular structures trap large quantity of air within the tubes. The air layers can prevent water drops entering the internal microtubule structure. This phenomenon agrees with the Cassie–Baxter model, leading to a superhydrophobic phenomenon.[42–44] The Cassie–Baxter model can be described by the following equation:

$$\cos\theta' = f_1 \cos\theta - f_2 \quad (1)$$

θ in the formula (1) refers to CA on the surface of the glass treated with PFOTS, θ' is the CA of surface treated with a dilute $[Ni(DMG)_2]$ and PFOTS; f_1 and f_2 are the proportions of the area occupied by the two media (liquid and gas) on the solid surface, separately (*i.e.*, $f_1 + f_2 = 1$). From eqn (1) it can be concluded that the f_2 number is 0.944, which reveals that atmosphere takes up 94.4% of the touch area when the superhydrophobic nominal gets to the liquid drop. It is worth mentioning that the superhydrophobicity is long lasting and can be kept after three months storage in air. The experiment data show the potential of the synthetic materials in the separation engineering.

To study the pH influence on wettability, we carried out corrosion reaction with acidic and basic aqueous solutions. The data were analysed, and results were shown in Fig. 5e. The CA first increased with the pH value, topped at pH = 7, then slowly decreased. The pH values of aqua pura and the contact angle had almost no influence. This can be seen from the figure that the CA values were greater than 156° when pH > 1. The glass is passivated against basic conditions after coating the $[Ni(DMG)_2]$. Chemical reactions are prohibited, leaving the surface anticorrosive to basic conditions. For further investigating the pH influence on wettability, the coatings were immersed in different PH solutions for 10 min. After that, the coating was allowed to air dry for twenty four hours at indoor temp, and then water contact angle was measured and results were shown in Fig. S6.† The changing tendency of the CA values were the same with different PH water dropped in the coatings. It can also be seen from the Fig. S6† that the CA values were all larger than 150° when the solutions pH > 1, topped at pH = 7. Stability test was also performed for the obtained superhydrophobic surfaces. After three months of storage at room temperature, water CA on the surface was still larger than 150°, which can demonstrate the coated surface is stable.

Unique liquid wettability of the $[Ni(DMG)_2]$ enable their application as coating materials to split oil–water mixtures. Video screenshot and video snapshots were taken from octane droplets dripped on the filter paper coated with the as-prepared powder. In Fig. 6, a drop of octane was soon absorbed within 2.321 s, which indicates that the film has a very good oil-filtering property.

Fig. 7b and d shows the SEM images of $[Ni(DMG)_2]$ films obtained by screen-printing technology on filter cloth and filter paper substrates, and corresponding pure filter cloth and filter paper are presented as a blank control group seen in Fig. 7a and c. From the low-resolution SEM images of Fig. 7a, the cloth

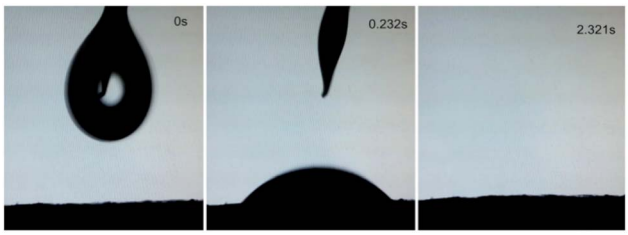

Fig. 6 Video snapshots of a drop of octane absorbed by the as-prepared $[Ni(DMG)_2]$ film.

mesh (200 μm × 200 μm mesh size) is distributed throughout the surface. After embellished by [Ni(DMG)$_2$], the mesh is uniformly covered by the microtubes (Fig. 7b). Such a coating changes considerable the wettability of the prepared sample. Similarly, fibers on filter paper (Fig. 7c) were evenly covered by the product microtubes (Fig. 7d) after being screen-printed. Iron wire mesh and copper grid are also employed as substrates, and the [Ni(DMG)$_2$] modified SEM images are depicted in Fig. S7b and d, with Fig. S7a and c† as the corresponding blank contrast. [Ni(DMG)$_2$] hollow microtubules distribute regularly on the iron wire mesh surface with 200 μm × 200 μm reseau, and 400 μm × 400 μm reseau on copper grid. The grid regulation of copper grid becomes smaller after printed [Ni(DMG)$_2$] and abundant [Ni(DMG)$_2$] hollow microtubules were printed on the copper grid, which may make a superior superhydrophobic property of [Ni(DMG)$_2$] films.

We further tested oil–water separation abilities of the [Ni(DMG)$_2$] covered substrates. Fig. 8 shows the separation process of the mixture on different substrates of filter paper, filter cloth, copper grid and iron mesh. Pour water (dyed with methylene blue) and dichloromethane (stained with Sudan Red III) into a beaker and mix, then pour on the coated film, that oil can pass through and then fall into the bottom of the device. However, water is not permissive due to the superhydrophobicity of the film (see details in the ESI mas S1–mas S5†). The blocked water was decanted into the measuring cylinder. Fig. 8b shows the device and the oil–water mixture with 10 mL oil and 10 mL water before filtration. After the oil–water separation at the coated filter cloth interface, Fig. 8c displays the content of mixed solution separated by filter clothe, and nearly 9.4 mL of water and 9.2 mL of oil are obtained. Such a process is visualized in Video S1,† and the segregation process was fast. Fig. 8d shows the content of the mixture solution through the filter paper after the separation. Approximately 8.0 mL dichloromethane and 9.8 mL H_2O were obtained, showing a very high separation efficiency of the superhydrophobic [Ni(DMG)$_2$] film. However, the segregation process was very slowly, and nearly ten minutes separation engineering

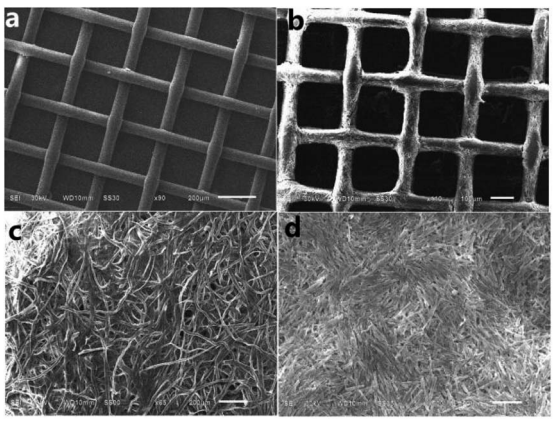

Fig. 7 SEM images of [Ni(DMG)$_2$] printed on filter cloth and filter paper (b and d); SEM images of pure filter cloth and filter paper without modifying by [Ni(DMG)$_2$] (a and c).

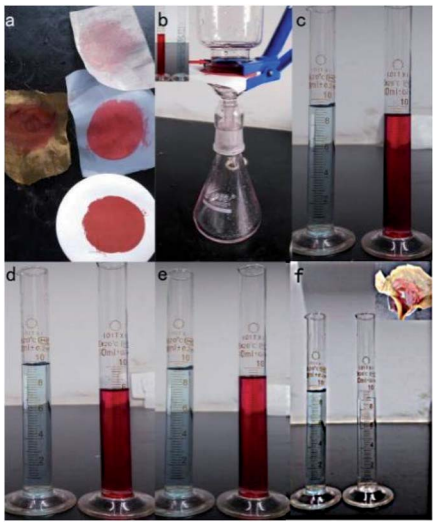

Fig. 8 The superhydrophobic and oleophobic film for application in separation oil from water: (a) [Ni(DMG)$_2$] printed on filter paper, filter cloth, copper grid, iron mesh substrate; (b) water (stained with methylene blue) and dichloromethane (stained with Sudan Red III) are poured into beaker and mixed for oil–water separation; (c–e) after filtration; (f) after separation methylene blue on copper grid ultraviolet lighted for 10 min.

was all over (Videos S2 and S3†). Fig. 8e shows approximately 9.3 mL of the water and 9.2 mL of the oil were collected when the product was printed on copper grid. It is worth mentioning that, the process of oil–water separation was executed through a folded copper grid on a beaker, the dichloromethane diffused quickly, passed through that copper grid, and then flowed into the becherglas underneath. Meanwhile, the water maintained above the copper grid, indicating outstanding oil–water segregation capacity (Video S4†). Also approximately 9.4 mL of the water and 9.3 mL of the oil were collected when the product was printed on iron mesh.

The water permeation coefficient (η/%) stands for the separation efficiency of the product. It reads η (%) = (m_1/m_0) × 100%, where m_1 on behalf of the weight of water after each oil–water splitting, and m_0 the weight of water in the beginning oil–water compound.[45,46] Through that equation, the isolation productivity of [Ni(DMG)$_2$] printed on filter cloth, copper grid, filter paper and iron mesh, water permeation coefficient were calculated to 94%, 93%, 98% and 94%, separately.

Supported by the previous experimental content, we further develop the prototypical design for wastewater treatment by combining the chemical activity and wettability of the as-prepared film. The oil–water separation was firstly carried out by using the coated Cu mesh as the filter. The methylene blue solution (5 mg L^{-1}) prevented on copper grid (as shown in Fig. 8f) was then transferred for photocatalysis. After UV light irradiated for only 10 min, the methylene blue become colourless (Fig. 8f). The dyed water is separated from oils and decontaminated.

The reusability and mechanical stability of the prepared [Ni(DMG)$_2$] film are also studied. The superhydrophobicity and

robustness of the prepared [Ni(DMG)$_2$] superhydrophobic film was assessed qualitatively by mechanical shear. The test was presented graphically in Fig. 9A. The as-prepared film surface printed on filter paper was scratched by a knife along a meshy path, and the wettability was confirmed through a water dropping test. As shown in Fig. 9A(a–f), the MB-dyed water droplets immediately rolled off from the film without wetting it after the surface was fixed to a tilting angle of 20°. No remaining MB dye can be observed on the surface neither (check out the detailed information in ESI mas S6†). The superhydrophobic surface possesses a good stability and satisfactory mechanical robustness.

For further study robustness of printed surfaces, filter paper and glass slide samples were sanded for wear testing (Fig. S8†). That as-prepared filter paper-based films were applied outward to the bottom of the weight of 20 g or 50 g. Placed the weight on a sandpaper of the P800 size and moved it ten centimeters in the longitudinal direction of the scale (Fig. S8a and b†), which was defined as a single wear cycle. It can be observed that the printed [Ni(DMG)$_2$] superhydrophobic coatings were not dropped down from the filter paper. At the same time, the measured CA values after 30 wear cycles indicated that the hydrostatic contact angles were 154° and 151° at 20 g and 50 g, respectively (for details see Videos S7 and S8†). The pictures of static water contact angles were shown in the inset of Fig. S8a and b.† The result indicates that the nominal of the coating reserved superhydrophobicity after the wear experiment. Also a glass slide film was used for detecting the robustness of printed surface, as shown in Fig. S8c.† The experimental procedure is consistent with the above experiments in general, but the weight was changed into 5 g and the film was abraded both longitudinally and transversely. From the detailed video of Video S9† it could be observed that some [Ni(DMG)$_2$] superhydrophobic coating was peeled off. We can summarize that the robustness performance of the product printed on glass slide should be further enhanced.

Besides the unique wettability, the [Ni(DMG)$_2$] coated film also indicated light stability and re-utilizing through ultraviolet photodegradation of quinoline blue. The [Ni(DMG)$_2$] coated glass was employed as the 'photocatalytic' system, and each reaction cycle fixed to 2 h. As clearly seeing from Fig. 9B, the photodegradation efficiency for quinoline blue decreased to 76% after four cycles of photocatalysis under UV radiation. This proves that the [Ni(DMG)$_2$] film possesses stable photoactivity, after cleaning the glass by aqua pura, the film can still be used again.

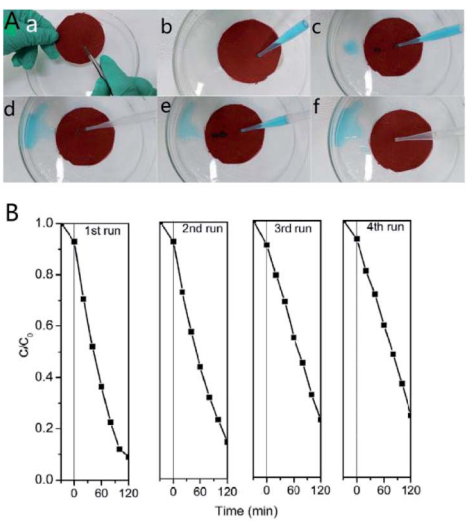

Fig. 9 (A) The knife-scratch test on the superhydrophobic surface of [Ni(DMG)$_2$] printed on filter paper (a–f); (B) repeated cycles of UV-induced photocatalytic degradation of quinoline blue over the [Ni(DMG)$_2$] film.

Conclusions

In conclusion, a practical water purification route was realized by using the [Ni(DMG)$_2$] microtubes as the oil–water separation media and photocatalyst. Synthesized *via* a simple precipitation method, unique morphology of the [Ni(DMG)$_2$] leads to specific the hydro- and oleo-wettability besides its selective photocatalytic properties. A superhydrophobic surface was achieved, due to its tubular structure and silanization with PFOTS. The hydrophobic mode is ascribed to the Cassie–Baxter model.[47] These experimental results have well confirmed superhydrophobicity of the [Ni(DMG)$_2$] coated surfaces and their excellent resistance to corrosion, and long durations. In addition, [Ni(DMG)$_2$] has a very good oil-absorbing property, which can also be applied to split oil–water mixtures. Combined with photocatalytic and water–oil separation abilities, the [Ni(DMG)$_2$] has been proved a multi-functional material for water purification in the complicated sewage situation of contaminated wastewater mixed with oils.

Conflicts of interest

There are no conflicts to declare.

Acknowledgements

The authors acknowledge with thanks the financial support of the National Natural Science Foundation of China (21601149) and Hunan 2011 Collaborative Innovation Center of Chemical Engineering & Technology with Environmental Benignity and Effective Resource Utilization. Feng Li thanks the support of China Scholarship Council.

Notes and references

1 H. Chen, S. Chen and X. Quan, Fabrication of TiO_2–Pt Coaxial Nanotube Array Schottky Structures for Enhanced Photocatalytic Degradation of Phenol in Aqueous Solution, *J. Phys. Chem. C*, 2008, **112**, 9285–9290.

2 S. W. Zhu, Q. G. Li, F. Li, T. H. Li and W. Cao, One-pot synthesis of Ag^+ doped $BiVO_4$ microspheres with enhanced photocatalytic activity *via* a facile hydrothermal method, *J. Phys. Chem. Solids*, 2016, **92**, 11–18.

3 J. M. Meichtry, C. Colbeau-Justin, G. Custo and M. I. Litter, TiO_2-photocatalytic transformation of Cr(VI) in the presence of EDTA: comparison of different commercial photocatalysts and studies by time resolved microwave conductivity, *Appl. Catal., B*, 2014, **144**, 189–195.

4 C. Sahoo, A. K. Gupta and A. Pal, Photocatalytic degradation of Methyl Red dye in aqueous solutions under UV irradiation using Ag^+ doped TiO_2, *Desalination*, 2005, **181**, 91–100.

5 D. Tian, X. Zhang, Y. Tian, Y. Wu, X. Wang, J. Zhai and L. Jiang, Photo-induced water–oil separation based on switchable superhydrophobicity–superhydrophilicity and underwater superoleophobicity of the aligned ZnO nanorod array-coated mesh films, *J. Mater. Chem.*, 2012, **22**, 19652–19657.

6 H. Yang, Y. Lan, W. Zhu, W. Li, D. Xu, J. Cui, D. Shen and G. Li, Polydopamine-coated nanofibrous mats as a versatile platform for producing porous functional membranes, *J. Mater. Chem.*, 2012, **22**, 16994–17001.

7 J. Li, L. Shi, Y. Chen, Y. Zhang, Z. Guo, B. Su and W. Liu, Stable superhydrophobic coatings from thiol-ligand nanocrystals and their application in oil/water separation, *J. Mater. Chem.*, 2012, **22**, 9774–9781.

8 P. Cieśla, P. Kocot, P. Mytych and Z. Stasicka, Homogeneous photocatalysis by transition metal complexes in the environment, *J. Mol. Catal. A: Chem.*, 2004, **224**, 17–33.

9 J. M. Joseph, R. Varghese and C. T. Aravindakumar, Photoproduction of hydroxyl radicals from Fe(III)-hydroxy complex: a quantitative assessment, *J. Photochem. Photobiol., A*, 2001, **146**, 67–73.

10 Z. G. Xiong and X. S. Zhao, Nitrogen-Doped Titanate-Anatase Core–Shell Nanobelts with Exposed {101} Anatase Facets and Enhanced Visible Light Photocatalytic Activity, *J. Am. Chem. Soc.*, 2012, **134**, 5754–5757.

11 M. Wang, J. Han, Y. Hu, R. Guo and Y. Yin, Carbon-Incorporated NiO/TiO_2 Mesoporous Shells with p–n Heterojunctions for Efficient Visible Light Photocatalysis, *ACS Appl. Mater. Interfaces*, 2016, **8**, 29511–29521.

12 P. Wang, D. Zhang, R. Qiu, Y. Wan and J. J. Wu, Green approach to fabrication of a super-hydrophobic film on copper and the consequent corrosion resistance, *Corros. Sci.*, 2014, **80**, 366–373.

13 P. Wang, D. Zhang and Z. Lu, Advantage of super-hydrophobic surface as a barrier against atmospheric corrosion induced by salt deliquescence, *Corros. Sci.*, 2015, **90**, 23–32.

14 J. Reedijk, Coordination chemistry beyond Werner: interplay between hydrogen bonding and coordination, *Chem. Soc. Rev.*, 2013, **42**, 1776–1783.

15 T. T. Lu, M. Yang, K. Yao, J. Xu and M. Lu, Metal free: a novel and efficient aerobic oxidation of toluene derivatives catalyzed by *N′*,*N″*,*N‴*,-trihydroxyisocyanuric acid and dimethylglyoxime in PEG-1000-based dicationic acidic ionic liquid, *Catal. Commun.*, 2012, **27**, 124–128.

16 L. L. Merritt Jr, X-Ray Structure Determinations, *Anal. Chem.*, 1953, **65**, 718.

17 A. Nezamzadeh-Ejhieh and M. Kabiri-Samani, Effective removal of Ni(II) from aqueous solutions by modification of nano particles of clinoptilolite with dimethylglyoxime, *J. Hazard. Mater.*, 2013, **260**, 339–349.

18 E. L. Bickerdike and H. H. Willard, Dimethylglyoxime for Determination of Nickel in Large Amounts, *Anal. Chem.*, 1952, **24**, 1026.

19 D. E. Williams, G. Wohlauer and R. E. Rundle, Crystal structures of nickel and palladium dimethylglyoximes[1], *J. Am. Chem. Soc.*, 1959, **81**, 755–756.

20 D. X. Li, D. J. Xu and Y. Z. Xu, Redetermination of bis-(dimethyl-glyoximato-κ2 *N*,*N′*)-nickel(II), *Acta Crystallogr., Sect. E: Struct. Rep. Online*, 2003, **59**, 1094.

21 A. Nezamzadeh-Ejhieh and Z. Shams-Ghahfarokhi, Photodegradation of Methyl Green by Nickel-Dimethylglyoxime/ZSM-5 Zeolite as a Heterogeneous Catalyst, *J. Chem.*, 2013, **2013**, 1–11.

22 J. Qin, B. Wang and X. Zhang, Controlled formation of $Ni(DMG)_2$ microrods/tubes by manipulating the kinetics of chemical reactions and their application in naked-eye sensors, *J. Nanosci. Nanotechnol.*, 2012, **12**, 6592–6595.

23 H. Wang, *In situ* Synthesis of Nickel-Dimethylglyoxime/Black Phosphorus Nanorods for Photocatalytic Hydrogen Production from Water Splitting, *Nano*, 2020, **10**, 2050125.

24 X. L. Li, X. Zhang, Z. Lia and Y. Qian, Synthesis and characteristics of NiO nanoparticles by thermal decomposition of nickel dimethylglyoximate rods, *Solid State Commun.*, 2006, **137**, 581–584.

25 X. M. Ni, Q. B. Zhao, Y. F. Zhang, J. M. Song, H. G. Zheng and K. Yang, Large scale synthesis and electrochemical characterization of hierarchical β-$Ni(OH)_2$ flowers, *Solid State Sci.*, 2006, **8**, 1312–1317.

26 X. M. Ni, Q. B. Zhao, J. Cheng, H. G. Zheng, B. B. Li and D. G. Zhang, High-yield Synthesis of Nickel Flowers from Nickel Hydroxide Precursor, *Chem. Lett.*, 2005, **34**, 1408–1409.

27 J. W. Ko, S. Y. Lee, H. D. Kim, K. H. Ha, J. H. Ahn and H. S. Chung, Fabrication of $Bi_2Sr_2CaCu_2O_x$/Ag superconducting tape using a screen-printing method, *J. Mater. Sci.*, 1994, **29**, 4639–4644.

28 Y. Chen, F. Li, W. Cao and T. H. Li, Preparation of Recyclable CdS Photocatalytic and Superhydrophobic Film with Photostability by Screen-printing Technique, *J. Mater. Chem. A*, 2015, **3**, 16934–16940.

29 N. Liu, Y. Z. Cao, X. Lin, Y. N. Chen, L. Feng and Y. Wei, A facile solvent-manipulated mesh for reversible oil/water separation, *ACS Appl. Mater. Interfaces*, 2014, **6**, 12821.

30 M. H. Tai, P. Gao, B. Y. L. Tan, D. D. Sun and J. O. Leckie, Highly efficient and flexible electrospun carbon–silica nanofibrous membrane for ultrafast gravity-driven oil–water separation, *ACS Appl. Mater. Interfaces*, 2014, **6**, 9393–9401.

31 C. X. Wang, T. J. Yao, J. Wu, C. Ma, Z. X. Fan, Z. Y. Wang, Y. R. Cheng, Q. Lin and B. Yang, Facile approach in fabricating superhydrophobic and superoleophilic surface for water and oil mixture separation, *ACS Appl. Mater. Interfaces*, 2009, **1**, 2613–2617.

32 I. F. Brucesmith, B. A. Zakharov, J. Stare, E. A. Boldyreva and C. R. Pulham, Structural Properties of Nickel

Dimethylglyoxime at High Pressure: Single-Crystal X-ray Diffraction and DFT Studies, *J. Phys. Chem. C*, 2014, **118**, 24705–24713.

33 L. Z. Pei, N. Lin, T. Wei and H. Y. Yu, Synthesis of manganese vanadate nanobelts and their visible light photocatalytic activity for methylene blue, *J. Exp. Nanosci.*, 2016, **11**(3), 197–214.

34 L. Luo, Y. Z. Li, J. T. Hou and Y. Yang, Visible photocatalysis and photostability of Ag_3PO_4 photocatalyst, *Appl. Surf. Sci.*, 2014, **319**, 332–338.

35 D. X. Li, D. J. Xu and Y. Z. Xu, Redetermination of bis-(dimethyl-glyoximato-κ2 *N*,*N*′)-nickel(II), *Acta Crystallogr., Sect. A: Found. Crystallogr.*, 2003, **59**, 1094–1095.

36 A. A. Dakhel and Y. Ali-Mohamed Ahmed, Electrical properties of thermally evaporated nickel-dimethylglyoxime thin films, *J. Phys. Chem. Solids*, 2005, **66**, 1080–1084.

37 K. Takeda, J. Hayashi, I. Shirotani, H. Fukuda and K. Yakushi, Structural, Optical, and Electrical Properties of One-Dimensional Bis(Dimethylglyoximato)nickel(II), $Ni(DMG)_2$ at High Pressure, *Mol. Cryst. Liq. Cryst.*, 2006, **460**, 131–144.

38 F. Lei and B. Yan, Morphology-Controlled Synthesis, Physical Characterization, and Photoluminescence of Novel Self-Assembled Pomponlike White Light Phosphor: Eu^{3+}-Doped Sodium Gadolinium Tungstate, *J. Phys. Chem. C*, 2009, **113**, 1074–1082.

39 S. Jadhav, S. Kulkarni and S. Quadri, Ultrasound Assisted Synthesis and Physiochemical Investigation of Nickel-Dimethyl Glyoxime Complex, *Journal of Chemistry and Chemical Sciences*, 2015, **5**, 311–316.

40 S. Loera-Serna, L. L. Nunez, J. Flores, R. Lopez-Simeon and H. I. Beltran, An alkaline one-pot metathesis reaction to give a $[Cu_3(BTC)_2]$ MOF at r.t., with free Cu coordination sites and enhanced hydrogen uptake properties, *RSC Adv.*, 2013, **3**, 10962–10972.

41 Y. Chen, F. Li, T. H. Li and W. Cao, Shape-controlled hydrothermal synthesis of superhydrophobic and superoleophilic $BaMnF_4$ micro/nanostructures, *CrystEngComm*, 2016, **18**, 3585–3593.

42 A. B. D. Cassie and S. Baxter, Wettability of porous surfaces, *Trans. Faraday Soc.*, 1944, **40**, 546.

43 S. Zhu, X. Yang, T. Li, F. Li and W. Cao, Phase and morphology controllable synthesis of superhydrophobic Sb_2O_3 *via* a solvothermal method, *J. Alloys Compd.*, 2017, **721**, 149–156.

44 L. Feng, Z. Y. Zhang, Z. H. Mai, Y. M. Ma, B. Q. Liu, L. Jiang and D. B. Zhu, A Super-Hydrophobic and Super-Oleophilic Coating Mesh Film for the Separation of Oil and Water, *Angew. Chem.*, 2004, **43**, 2012–2014.

45 Q. M. Pan, M. Wang and H. B. Wang, Separating small amount of water and hydrophobic solvents by novel superhydrophobic copper meshes, *Appl. Surf. Sci.*, 2008, **254**, 6002–6006.

46 J. Li, M. Liu, L. Shi and Z. Guo, Stable underwater superoleophobic conductive polymer coated meshes for high-efficiency oil–water separation, *RSC Adv.*, 2015, **5**, 33077–33082.

47 T. Pisuchpen, N. Chaim-ngoen, N. Intasanta, P. Supaphol and V. P. Hoven, Tuning Hydrophobicity and Water Adhesion by Electrospinning and Silanization, *Langmuir*, 2011, **27**, 3654–3661.